SARS-CoV-2 activates ER stress and Unfolded protein response

Livia Rosa-Fernandes[1,2#], Lucas C. Lazari[1#], Janaina Macedo da Silva[1#], Vinicius de Morais Gomes[1], Rafael Rahal Guaragna Machado[3], Ancely Ferreira dos Santos[4], Danielle Bastos Araujo[3], João Vitor Paccini Coutinho[1], Gabriel Santos Arini[4], Claudia B. Angeli[1], Edmarcia E. de Souza[5], Carsten Wrenger[5], Claudio R. F. Marinho[2], Danielle B. L. Oliveira[3], Edison L. Durigon[3,6], Leticia Labriola[4], Giuseppe Palmisano[1*]

1. GlycoProteomics Laboratory, Department of Parasitology, ICB, University of São Paulo, Brazil

2. Laboratory of Experimental Immunoparasitology, Department of Parasitology, ICB, University of São Paulo, Brazil

3. Laboratory of Clinical and Molecular Virology, Department of Microbiology, ICB, University of São Paulo, Brazil

4. Department of Biochemistry, Institute of Chemistry, University of São Paulo, Brazil

5. Unit for Drug Discovery, Department of Parasitology, ICB, University of São Paulo, Brazil

6. Scientific Platform Pasteur USP, Sao Paulo, Brazil

# These authors share first authorship

* To whom correspondence should be addressed: Prof. Giuseppe Palmisano, Glycoproteomics Laboratory, Department of Parasitology, ICB, University of São Paulo, Brazil, Av. Prof. Lineu Prestes, 1374, 05508-900 - São Paulo – SP – Brazil, Tel: + 55-11-99920-8662, palmisano.gp@gmail.com, palmisano.gp@usp.br

ABSTRACT

Coronavirus disease-2019 (COVID-19) pandemic caused by the SARS-CoV-2 coronavirus infection is a major global public health concern affecting millions of people worldwide. The scientific community has joint efforts to provide effective and rapid solutions to this disease. Knowing the molecular, transmission and

clinical features of this disease is of paramount importance to develop effective therapeutic and diagnostic tools. Here, we provide evidence that SARS-CoV-2 hijacks the glycosylation biosynthetic, ER-stress and UPR machineries for viral replication using a time-resolved (0-48 hours post infection, hpi) total, membrane as well as glycoproteome mapping and orthogonal validation. We found that SARS-CoV-2 induces ER stress and UPR is observed in Vero and Calu-3 cell lines with activation of the PERK-eIF2α-ATF4-CHOP signaling pathway. ER-associated protein upregulation was detected in lung biopsies of COVID-19 patients and associated with survival. At later time points, cell death mechanisms are triggered. The data show that ER stress and UPR pathways are required for SARS-CoV-2 infection, therefore representing a potential target to develop/implement anti-CoVID-19 drugs.

Keywords: Coronavirus, ER stress, Unfolded protein response, SARS-CoV-2, COVID-19, proteomics, Vero CCL-81, CALU-3

INTRODUCTION

Coronavirus Disease 19 (COVID-19) is caused by severe acute respiratory syndrome coronavirus 2 (SARS-CoV-2) [1], an enveloped RNA virus belonging to the family *Coronaviridae* in the subfamily *Orthocoronavirinae* [2]. Common symptoms of human infection are dry cough, sore throat and fever; however, a percentage of the patients can develop organ failure, septic shock, pulmonary edemas, severe pneumonia and Acute Respiratory Distress Syndrome, complications that can be fatal [3]. Considering the fast increase in the infection numbers and the outbreaks of SARS-CoV-2 in other countries, on 30th January of 2020 the World Health Organization (WHO) declared COVID-19 to be a Public Health Emergency of International Concern and warned that countries with vulnerable health care systems would be at high risk [3].

Understanding host-pathogen interactions and the host response to viral infection are important to develop new strategies to treat, prevent and diagnose COVID-19 [4]. The host-pathogen dynamics is the key to infection control and minimize spread, incidence, prevalence and mortality [5–8]. In the host cell, viral

proteins are processed through the endoplasmic reticulum (ER) and Golgi apparatus shaping the glycosylation level (especially N-linked glycans) of each site and regulating their folding[9]. This post-translational modification is often used by viruses to evade immune recognition, to increase receptor binding, infectivity, viral release, virulence and to increase viral replication [10–12]. Therefore, glycosylation process is the subject of numerous studies and often used as therapeutic target to treat viral infections [13]. One strategy is to target the host glycosylation machinery to pharmacologically disrupt viral glycoproteins folding, being the inhibitors of N-linked glycosylation one of the most tested agents for antiviral use [14]. In particular, recent reports have shown that not only the targeting of host machinery but a direct modification in glycosylation levels of viral glycoproteins could impair viral infection/replication of SARS-Cov-2, thus indicating that targeting this process is a promising strategy to reduce SARS-CoV-2 infection.

Viral infections typically lead to an increase in protein synthesis that can overwhelm the ER folding capacity, which may result in unfolded protein accumulation resulting in ER stress [15]. To reduce this type of stress, the cell activates signaling pathways known as unfolded protein response (UPR), that reduces the overall protein synthesis, increases ER's folding capacity and targets misfolded proteins to proteasome degradation [16]. UPR consists of three signaling pathways activated by the transmembrane protein sensors IRE1, PERK and ATF6.

Briefly, IRE1 branch activation causes the mRNA splicing of a potent transcription factor, XBP1, which induces the expression of genes that will act in ER stress response. The first step in the PERK branch activation includes the increase on its phosphorylation state, which promotes the release of ER chaperone BiP as well as the phosphorylation of the transcriptional factor eIF2α, which will then upregulate ATF4 expression. This signaling pathway culminates with protein synthesis attenuation and selective induction of translation of ER chaperones and UPR-related transcriptional factors. Finally, the accumulation of unfolded proteins causes ATF6 release from the ER membrane allowing its traffic to the Golgi apparatus, where it will be activated by cleavage and consequently

lead to upregulation of genes encoding for ER chaperones and components necessary for degradation of unfolded proteins [17].

Recognizing the biomolecular features that facilitate infection and which host-mediated mechanisms the pathogen uses to favor its replication and transmission are substantial to achieve disease control and prevention[18]. Quantifying and analyzing the temporal changes in host and viral proteins over the biological processes of infection could provide valuable information about the virus-host interplay [19]. Here we applied a temporal and spatial proteome analysis combined with assessment of N-deglycoproteome to depict the host response to SARS-CoV-2 infection. We demonstrated that SARS-CoV-2 induces ER stress response, UPR and modulation of glycosylation machinery in the host cell. ER-associated transcripts upregulation was also detected in lung biopsies of COVID-19 patients and associated with higher survival. We also show that sustained infection prolonged the effects of ER-stress and UPR, leading to cell death related to necroptosis and caspase induced apoptosis pathways.

MATERIALS AND METHODS

Cell lines, SARS-CoV-2 and infection assays

Vero cell line (ATCC CCL-81) were maintained in DMEM medium supplemented with 10% (v/v) FBS, 4.5 g/L glucose, 2 mM L-glutamine, 1 mM sodium pyruvate, 100 U/mL penicillin-streptomycin and 1.5 g/L NaHCO3 at 37°C with 5% CO2. Calu-3 cells (ATCC HTB-55) were maintained in DMEM medium supplemented with 20% (v/v) FBS, 1% (v/v) nonessential amino acids, 4.5 g/L glucose, 2 mM L-glutamine, 1 mM sodium pyruvate, 100 U/mL penicillin-streptomycin and 1.5 g/L NaHCO3 at 37 °C with 5% CO2.

SARS-CoV-2 isolate (HIAE-02: SARS-CoV-2/SP02/human/2020/BRA (GenBank accession number MT126808) [20] was used to infect Vero CCL-81 and Calu-3 cells with multiplicity of infection (MOI) of 0.02. Following adsorption in DMEM with 2.5% FBS for 1h, fresh medium was added, and cells were further incubated at 37 °C and 5% CO2 for different time points (2, 6, 12, 24 and 48h). After the designated incubation time, cell lysates were retrieved in 1% sodium

deoxycholate (SDC) in phosphate buffered saline solution with Protease Inhibitor Cocktail (cOmplete, Roche) buffer, 0.1M Na2CO3 with Protease Inhibitor Cocktail (cOmplete, Roche) buffer or 8M Urea with Protease Inhibitor Cocktail (cOmplete, Roche) buffer, according to the follow-up application. Aliquots of cells and supernatants were collected at the different time points for virus RNA copy number quantification by reverse transcription-quantitative polymerase chain reaction (RT-qPCR), targeting the E gene [21]. The assay was reproduced in two independent experiments and expressed by standard error of the mean (SEM). Graphics and SEM were done using GraphPad Prism software version 8.1 (GraphPad Software, San Diego, USA).

All assays were conducted in triplicates in a BSL-3 facility at the Institute of Biomedical Sciences, University of Sao Paulo, under the Laboratory biosafety guidance related to coronavirus disease (COVID-19): Interim guidance, 28 January 2021 (https://www.who.int/publications/i/item/WHO-WPE-GIH-2021.1).

Total proteome analysis (cell lysis and trypsin digestion)

SARS-CoV-2-infected and mock-infected control cells were lysed in 1% sodium deoxycholate (SDC), 1× PBS and 1× protease inhibitor cocktail (Sigma-Aldrich) and probe tip sonicated for three cycles for 20 s and intervals of 30 s on ice [22]. Proteins were reduced with 10 mM DTT for 30 min at 56 °C and alkylated with 40 mM IAA for 40 min at room temperature, in the dark. Proteins were quantified using NanoDrop 2000 spectrophotometer (Thermo Scientific) before sequencing grade porcine trypsin (Promega) was added to a 1:50 ratio. The digestion, which proceeded for 16 h at 37 °C, was blocked by adding TFA 1% (v/v) final concentration before the SDC was removed from the solution by centrifugation at 10000 x g for 10 min [22]. Tryptic peptides were desalted using reversed phase C18 microcolumns before LC-MS/MS analysis.

Microsomal membrane proteome analysis (cell lysis and trypsin digestion)

Microsomal membrane protein fraction was isolated as previously described [23,24]. Briefly, cells were lysed in 100 mM Na_2CO_3, pH 11 containing protease inhibitors cocktail (Sigma-Aldrich) by sonication using three rounds of probe-tip sonication

at 40% output for 20 s with 30 s resting on ice. The lysates were incubated at 4°C with gentle rotation for 1.5 h followed by ultracentrifugation at 100000 x g for 1.5 h. After ultracentrifugation, the pellets were recovered and washed with 100mM triethylammonium bicarbonate (TEAB) and re-dissolved in 8 M urea in 50mM TEAB. Protein concentration determination was performed using Qubit fluorescent assay (Invitrogen). The solubilized membrane pellets were reduced and alkylated as described above. Urea was diluted to 0.8 M with 50mM TEAB and proteins were digested with trypsin at an enzyme to substrate ratio of 1:50 for 16 h at room temperature. Tryptic peptides were purified using Oligo R3 reversed phase SPE micro-column [25].

Glycopeptide enrichment and PNGase F deglycosylation

Tryptic glycopeptides obtained from microsomal membrane proteins were enriched using HILIC SPE as previously described [26,27]. Briefly, dried peptides were reconstituted in 100 µL loading and washing buffer containing ACN 80% (v/v) in TFA 1% (v/v). Peptides were loaded onto a primed custom-made HILIC SPE micro-column packed with PolyHYDROXYETHYL A™ resin (PolyLC Inc). The HILIC SPE columns were then washed in 100 µL loading and washing buffer. The enriched glycopeptides were eluted with TFA 1% (v/v) followed by 25 mM NH_4HCO_3 and finally ACN 50% (v/v). The three eluted fractions were then combined, dried by vacuum centrifugation and purified on a primed Oligo R3 reversed phase SPE micro-column. The enriched glycopeptides were resuspended in 50 mM Ambic, pH 7.5 and de-N-glycosylated using 500 U N-glycosidase F (PNGase F, New England Biolabs) for 12 h at 37°C. After incubation, the de-N-glycosylated were purified on a primed Oligo R3 reversed phase SPE micro-column, before LC-MS/MS analysis.

LC-MS/MS proteomics analysis

Tryptic peptides were analyzed by nanoflow LC-MS/MS analysis. The nLC-MS/MS analysis was performed using an Easy nano LC1000 (Thermo) HPLC coupled with an LTQ Orbitrap Velos (Thermo). Peptides were loaded on a C18 EASY-column (2cm x 5 µm x 100 µm; 120 Å pore, Thermo) using a 300 nL/min

flow rate of mobile phase A (0.1% formic acid) and separated in a C18 PicoFrit PepMap (10 cm x 10 µm x 75 µm; 135 Å pore, New Objective), over 105 minutes using a linear gradient 2-30 % followed by 20 min of 30-45% of mobile phase B (100% ACN; 0,1% formic acid). The eluted peptides were ionized using electrospray. The top 20 most intense precursor ions with charge-state ≥ 2 were fragmented using CID at 35 normalized collision energy and 10 ms activation time. The MS scan range was set between 350-1800 m/z, the MS scan resolution was 60.000, the MS1 ion count was 1x10e6 and the MS2 ion count was 5x10e4. The mass spectrometry proteomics data have been deposited to the ProteomeXchange Consortium (http://proteomecentral.proteomexchange.org) via the PRIDE partner repository [28].

Database Search and Statistical Analysis

Raw data were searched using Proteome Discoverer computational platform v2.3.0.523 (PD) using the Sequest search engine. The parameters used for database search were *Chlorocebus* (20,699 entries downloaded on 12/2020) proteome databases supplemented with the UniProt SARS-CoV-2 proteome and with the common contaminants. Trypsin as cleavage enzyme, two missed cleavages allowed, carbamidomethylation of cysteine as fixed modification, oxidation of methionine, and protein N-terminal acetylation as variable modifications. Asparagine and glutamine deamidation were included as variable modifications in the de-glycoproteome data. In the Proteome Discoverer platform, the percolator, peptide, and protein validator nodes were used to calculate PSMs, peptides, and proteins FDR, respectively. FDR less than 1% was accepted at protein level. Protein grouping was performed using the strict parsimony principle. Label-free quantification was performed using the extracted ion chromatogram area of the precursor ions. Protein quantification normalization and roll-up were performed using unique and razor peptides and excluding modified peptides. Differentially regulated proteins between the three conditions were selected using *t test* with a post-hoc background-based adjusted p-value <0.05 for multiple hypothesis correction [29].

Bioinformatics analysis

Gene ontology (GO) was performed using the g: profiler tool and GOplot package [30], available in Bioconductor. A q-value threshold of 0.05 was used, corrected by the Benjamini-Hochberg method [31]. Enriched pathways were determined by Reactome and KEGG platform (q-value < 0.05)[32]; complementary analyses were performed using the ReactomeFIPlugIn app [31]. Protein's subcellular locations were determined by UniProt release 12.4 (https://www.uniprot.org/news/2007/10/23/release). The "Peptides" package [33] was used to determine the hydropathy score of glycopeptides and the "mixOmics" package [34] was used to integrate the data for total, membrane, and deglycoproteome. Complementary analyses were performed using Perseus, ggplot2 package, Graphpad prism v.8, and RStudio software.

Structural analysis of identified peptides

Structural data for full-length SPIKE protein was retrieved from the CHARMM-GUI coronavirus repository, based on the model of Wrapp et al [35], while ORF8 protein structure was downloaded from PDB [36]. Peptides identified through MS data analysis were searched in the protein to better visualize their regions using PyMOL 2.4.1

Western blotting

Cells were lysed in SDC buffer containing protease (Roche, Basel, Switzerland) and phosphatase (Sigma-Aldrich) inhibitor cocktails. Proteins (10ug of each cell lysate) were separated by SDS-PAGE and electro transferred onto PVDF membranes. They were subsequently blocked in a solution containing 5% milk in PBS-Tween 0.1% (v/v) for 1h at room temperature (RT). Primary antibodies were diluted in the blocking solution (**Table 1**) and were incubated overnight at 4°C. Membranes were washed three times in PBS-Tween (0.1%) and then incubated at RT for 1h with HRP-labeled secondary antibodies, diluted in a solution of 0,1% BSA in PBS-Tween 0.1% (v/v). Monoclonal anti-alpha-tubulin clone B-5-1-2 antibody (T5168, Sigma-Aldrich) was used as the loading control. For phospho-protein quantification, the membranes were stripped, blocked and reprobed using a solution containing the corresponding anti-fosfospecific antibody. Proteins were

visualized by using enhanced chemiluminescence (Millipore Corporation, Billerica, MA, USA). Images were acquired using Uvitec Image System (Cleaver Scientific Limited, Cambridge, UK). Quantitative densitometry was carried out using the ImageJ software (National Institutes of Health). The volume density of the chemiluminescent bands was calculated as integrated optical density × mm2 using ImageJ Fiji. Phosphorylated proteins densitometry values were divided by the total protein values and the α-tubulin antibody was used as the normalizer of the amount of proteins applied in the gel. At least three independent experiments were performed for each cell type and condition.

Table 1: List of primary antibodies used for protein detection by Western blot.

Protein	Company	Catalog	Dilution
Phospho(S345) MLKL	Abcam	ab196436	1:1000
MLKL	Abcam	ab184718	1:1000
GPX4	Abcam	ab125066	1:1000
NRF2	Abcam	ab137550	1:1000
Phospho-PERK (Thr980)	Cell Signaling	#3179S	1:500
PERK	Cell Signaling	#3192	1:1000
phospho-eIF2α (S51)	Cell Signaling	#3597S	1:1000
eIF2α	Cell Signaling	#5324	1:1000
ATF4	Cell Signaling	#11815	1:1000
phospho-IRE1α (S724)	Abcam	ab48187	1:1000
IRE1α	Cell Signaling	#3294	1:1000
XBP1s	Cell Signaling	#12782	1:1000
ATF6	Abcam	ab11909	1:1000
CHOP	Cell Signaling	#2895	1:500
BIP	Cell Signaling	#3183	1:1000
Clivead-CASP3 (Asp175)	Cell Signaling	#9661L	1:500
CASP3	Cell Signaling	#9668S	1:500
CASP9	Cell Signaling	#9508S	1:1000
Alpha-tubulin clone B-5-1-2	Sigma-Aldrich	T5168	1:10.000
Anti-rabbit	Vector Laboratories	PI1000	1:1000
Anti-mouse	Vector Laboratories	PI2000	1:1000

Statistical analysis

All western blot results were analyzed for Gaussian distribution and passed the normality test (the number of independent experiments was chosen to present a normal distribution). The statistical differences between group means were tested

by One-way ANOVA followed by Tukey´s post-test for multiple comparisons. A value of $p<0.05$ was considered as statistically significant in all analysis. Results are presented as mean ± S.E.M. Each dot represents an independent experiment.

RNA-seq data reanalysis

The fastq files were downloaded from the https://sra-explorer.info/ platform with the BioProject accession number PRJNA646224 [37] and processed on the Galaxy server [38]. The 'FastQC' module was used to report the quality reads, following by the trimmed using Trim Galore (v. 0.4.3.1) set to the single-end library. The Trim Galore output sequences were aligned to the human reference genome hg38 using the HISAT2 (Galaxy Version 2.1.0+galaxy7) platform. A count table was generated using the htseq-count (Galaxy Version 0.9.1). The differently regulated genes were analyzed by the limma, Glimma, edgeR, and Homo.sapiens packages applying a cut-off of |log2FC|>1 and a p-adjusted value <0.05 (Benjamini-Hochberg).

RESULTS

To identify molecular pathways affected by viral-host interplay on the course of SARS-CoV-2 infection, a spatio-temporal MS-based quantitative approach comprised of proteome, membranome and N-deglycoproteome of SARS-CoV-2 infected Vero cells was conducted at 2, 6, 12 and 48 hpi. The membranome refers to the analysis of microsomal-enriched proteins while the N-deglycoproteome refers to the analysis of formerly N-linked glycopeptides associated proteins. Validation of differentially expressed proteins was performed in human epithelial lung cells (Calu-3) by western blotting and *in silico* transcriptome analysis of lung biopsies from COVID-19 patients and controls (**Figure 1A**).

A total of 1842 proteins were identified and quantified in the proteome analysis (**Supplementary Data S1**). Eight viral proteins were identified, being three structural proteins (M, S and N) and 5 non-structural proteins (ORF3a, ORF6, ORF9b, ORF7a and ORF1ab) (**Figure 1B, Supplementary Data S1**). These proteins increased over time showing a steeper upsurge already after 6 hpi, in agreement with the qPCR data (**Supplementary Figure 1**). Respectively, PCA

analysis of quantitative host-proteome features showed a clear separation between early (2 and 6 hpi) and late (24 and 48 hpi) infection times (**Figure 1C**). Host proteome regulation varied across time, showing preponderant downregulation until 48 hpi, when most regulated proteins were up-regulated compared to control (**Figures 1D and E, Supplementary Data S1**). For the time-points of 2, 6, 12, 24 and 48 hpi, we identified a total of 110, 79, 117, 111 and 184 regulated proteins, respectively (**Figure 1E, Supplementary Data S1**).

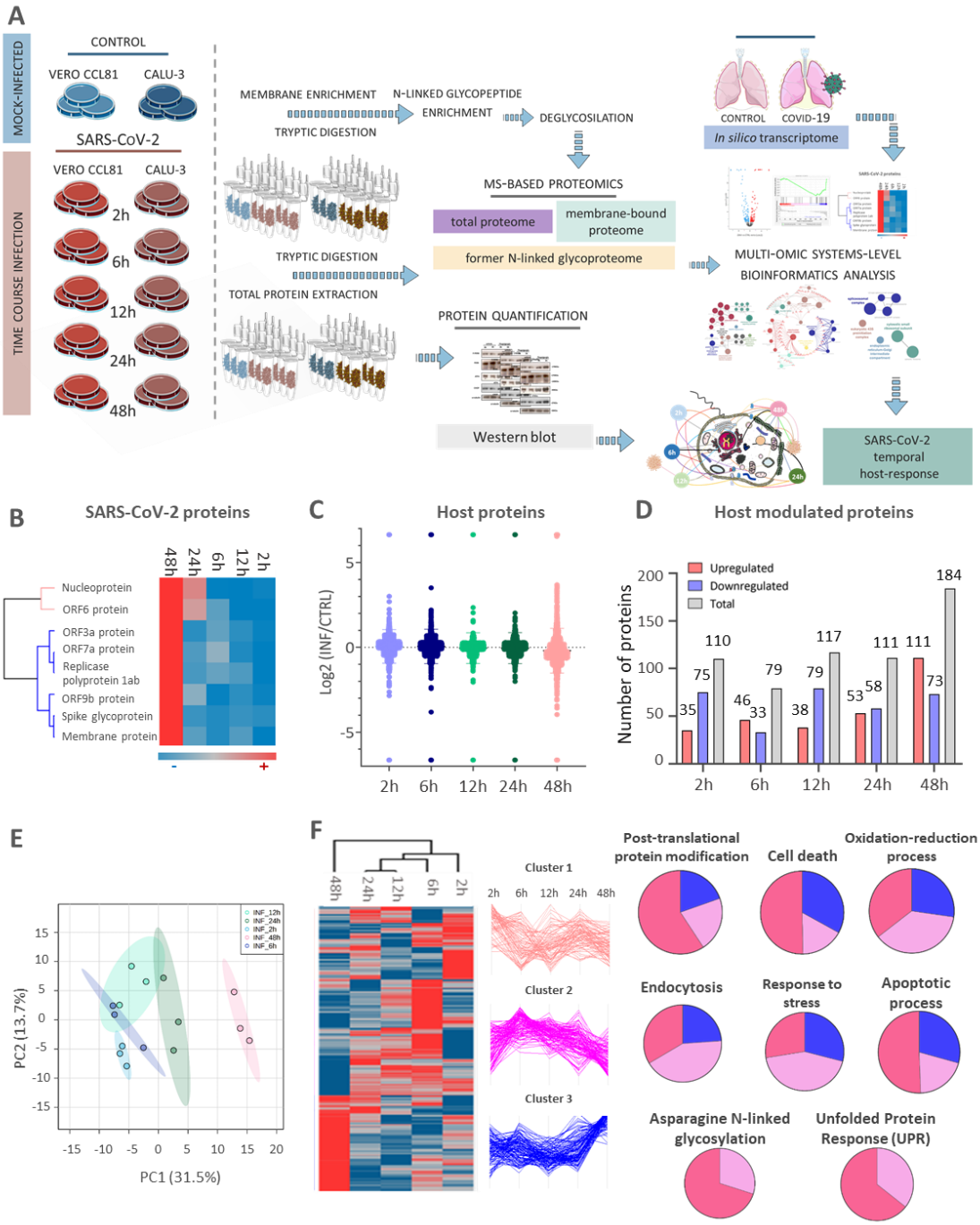

Figure 1. **Time-resolved proteome modulation upon SARS-CoV-2 infection**. Experimental approach applied to access spatiotemporal host-response to SARS-CoV-2 infection included evaluation of proteome, membranome and N-deglycoproteome of infected cells combined with WB protein quantification and transcriptome analysis of lung tissue of COVID-19 patients (A). Heatmap of SARS-CoV-2 viral proteins expression. Red and blue colors indicate high and low expression, respectively (B); Principal component analysis of quantitative proteome changes during infection(C); Quantitative proteome profile of Vero cells infected with SARS-CoV-2 after 2h, 6h, 12h, 24h, and 48h. The log2 ratio of infected vs control is shown (D); Vero cell proteins differentially regulated between the control (CTRL) and infected (INF) paired groups (q-value <0.05) at different time points. Red, blue and grey bars indicate up, down and total regulated proteins, respectively (E); Differentially regulated host proteins in at least one time point. Proteins were grouped into clusters associated with early, middle, and late events, respectively. Representation of enriched biological processes (BP) per cluster (q-value <0.05) (F).

To understand the global changes taking place in the host proteome during viral infection, we analyzed the differences in protein levels over time in a system-wide manner (**Figure 1F**). The host proteome already changed in the early time-points (2 and 6 hpi), but 48 hpi showed most extensive modulation. We identified three main clusters which contained proteins that participate in several key biological processes for early, middle and late times of host response expression profile (**Figure 1F**). Our analysis revealed processes related to post-translational protein modification, cell death, oxidation-reduction, endocytosis, response to stress, unfolded protein response (UPR), apoptosis and N-linked glycosylation (**Figure 1F, Supplementary Data S1**). Interestingly, assessment of protein subcellular location showed that while ER-related proteins more representative in the early time-points than at 48 hpi, the opposite pattern was observed for Nucleus-related proteins (**Figure 2A**). We found the expression of proteins associated with glycosylation biosynthesis modulated through the course of infection (**Figure 2B, Supplementary Data S1**). Of note are the ones related to nucleotide sugar biosynthesis, proteoglycans and glycosyltransferases (**Figure 2C)** besides intracellular membrane-bound organelle, endomembrane system and extracellular region cellular location **(Figure 2D).** Moreover, biological processes and pathways related to stress response and Asparagine N-linked Glycosylation were already observed at 2 hpi. In addition, alteration of proteins involved in UPR regulation were observed at 6 hpi (**Figure 2E and F**). These data indicate a remodeling of the host glycoproteome upon SARS-CoV-2 infection.

Since we observed glycosylation processes and multiple biological processes involving ER and membrane proteins, we proceeded with the evaluation of membranome and N-deglycoproteome (**Figure 3A, Supplementary Data Set 2**). We found 323 proteins identified in all three approaches, showing an increase in proteome coverage by enriching for glycosylated and membrane proteins (**Figure 3A**). As observed in the proteome, the number of regulated proteins in the membranome also increased over time, and at 48 hpi the number of down-regulated proteins was higher than the up-regulated ones (**Figure 3B**). Host proteins associated to glycoconjugate biosynthesis were mapped (**Figure 3C**). Moreover, we identified 1,037 N-deglycopeptides from the host (**Figure 3D, Supplementary Data Set 2**), being 545 regulated ones belonging to 338 N-deglycoproteins (**Supplementary Data Set 2**). The number of regulated N-deglycopeptides increased over time, but differently from the total proteome, most of which were downregulated at 48 hpi (**Figure 3E, Supplementary Data Set 2**). Expression pattern of the regulated N-deglycopeptides indicated a formation of three clusters (**Figure 3F, Supplementary Data Set 3**). In the first cluster an increase in the N-deglycopeptide abundance was observed over time while in cluster 3 there was a decrease. The hydropathy score associated to N-deglycopeptides in cluster 3 was significantly higher than the ones in cluster 1 **(Figure 3G**).

Moreover, abundance of viral proteins identified together with host membrane increased sharply at 48 hpi, as expected due to viral replication (**Figure 3H**). We were also able to quantify 20 SARS-CoV-2 formerly N-linked glycopeptides, being 2 mapped to nucleoprotein, 1 to ORF8 protein and 17 to spike glycoprotein (**Figures 3I and J, Supplementary Data Set 2**). We modelled the spike protein and highlighted the identified glycosylation sites and their abundance change during infection (**Supplementary Figure 2**). Mapping the identified N-deglycopeptides associated to spike (P0DTC2) and ORF8 (P0DTC8) proteins surface illustrated possible sites crucial for their function (**Supplementary Figure 2**).

Functional enrichment analysis of host regulated membrane proteins showed cell death, stress response and transport related processes already modulated at 2 hpi. Processes and pathways related to post-translational modification and asparagine N-linked glycosylation were observed at 12 hpi, while apoptosis, protein folding and oxidative stress were among up-regulated processes at 24 hpi and 48 hpi (**Supplementary Data Set 3**~~).~~

By performing an integrated analysis of all MS-based approaches, we identified the formation of four clusters (**Figures 4A and B, Supplementary Data Set 3**), demonstrating again that ER-related processes and cell death are being regulated during infection (**Figure 4C and D, Supplementary Data Set 3**). ER-related processes were mostly regulated at intermediate time-points, similar to proteome findings. To visualize the regulated processes, we built protein networks for all clusters with regulated proteins found in the merged dataset. We found that Cell death, UPR and Response to endoplasmic reticulum stress shared common nodes (**Figure 4 E-I**).

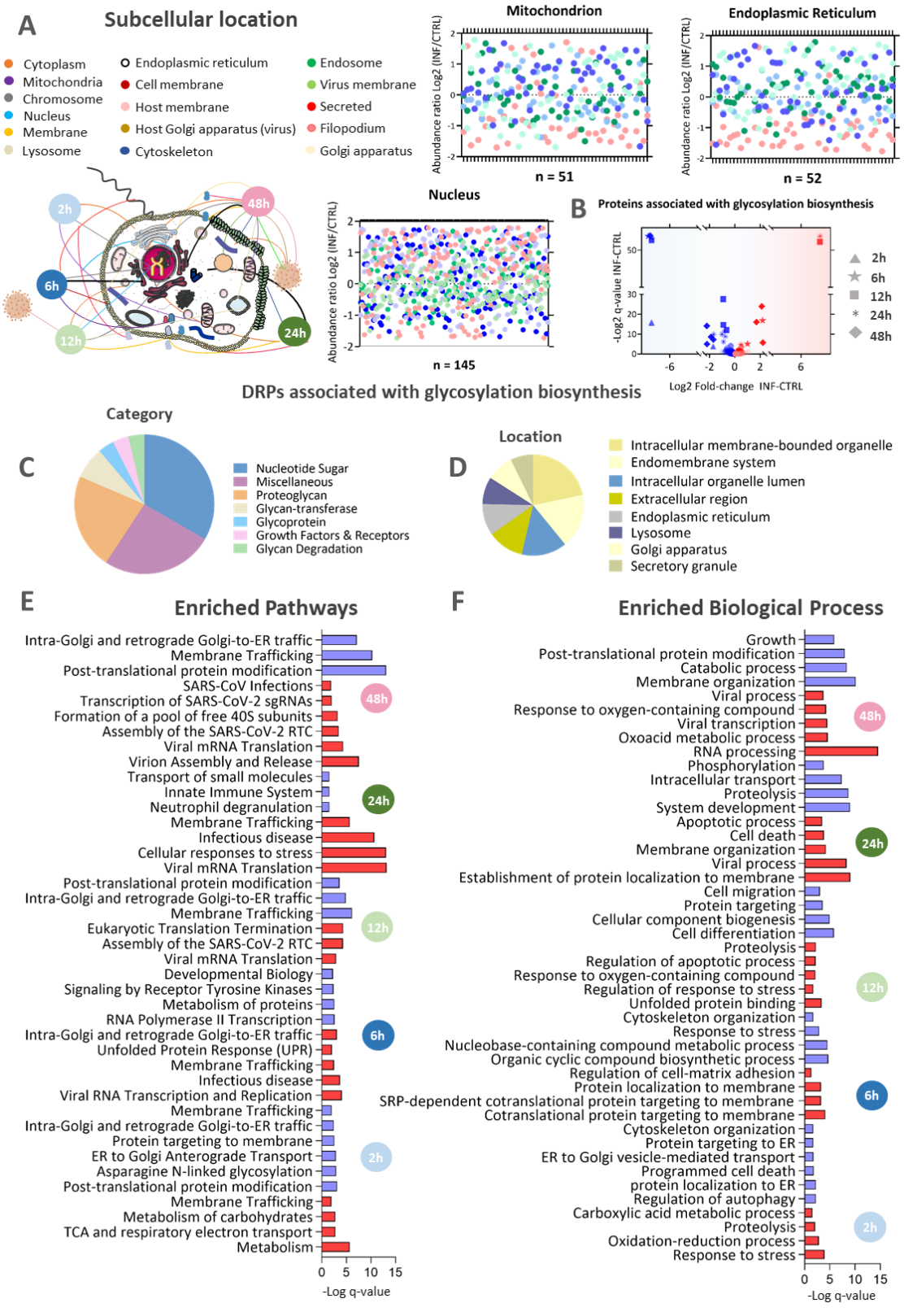

Figure 2. Time-resolved functional analysis of differentially expressed proteins upon SARS-CoV-2 infection. Abundance ratio (log2 infected vs control) of differentially regulated proteins associated to nucleus, mitochondria and ER according to infection time (A); Volcano plot of proteins associated to the glycosylation biosynthesis modulated in SARS-CoV-2-infected Vero cells vs control Up and downregulated proteins are

385 represented in red and blue, respectively (B); Category (C) and subcellular location (D)
386 of differently regulated proteins associated to the glycosylation biosynthesis. Enriched
387 pathways (E) and biological processes (BP) (F) at 2, 6, 12, 24 and 48 hpi (q-value <0.05).

388

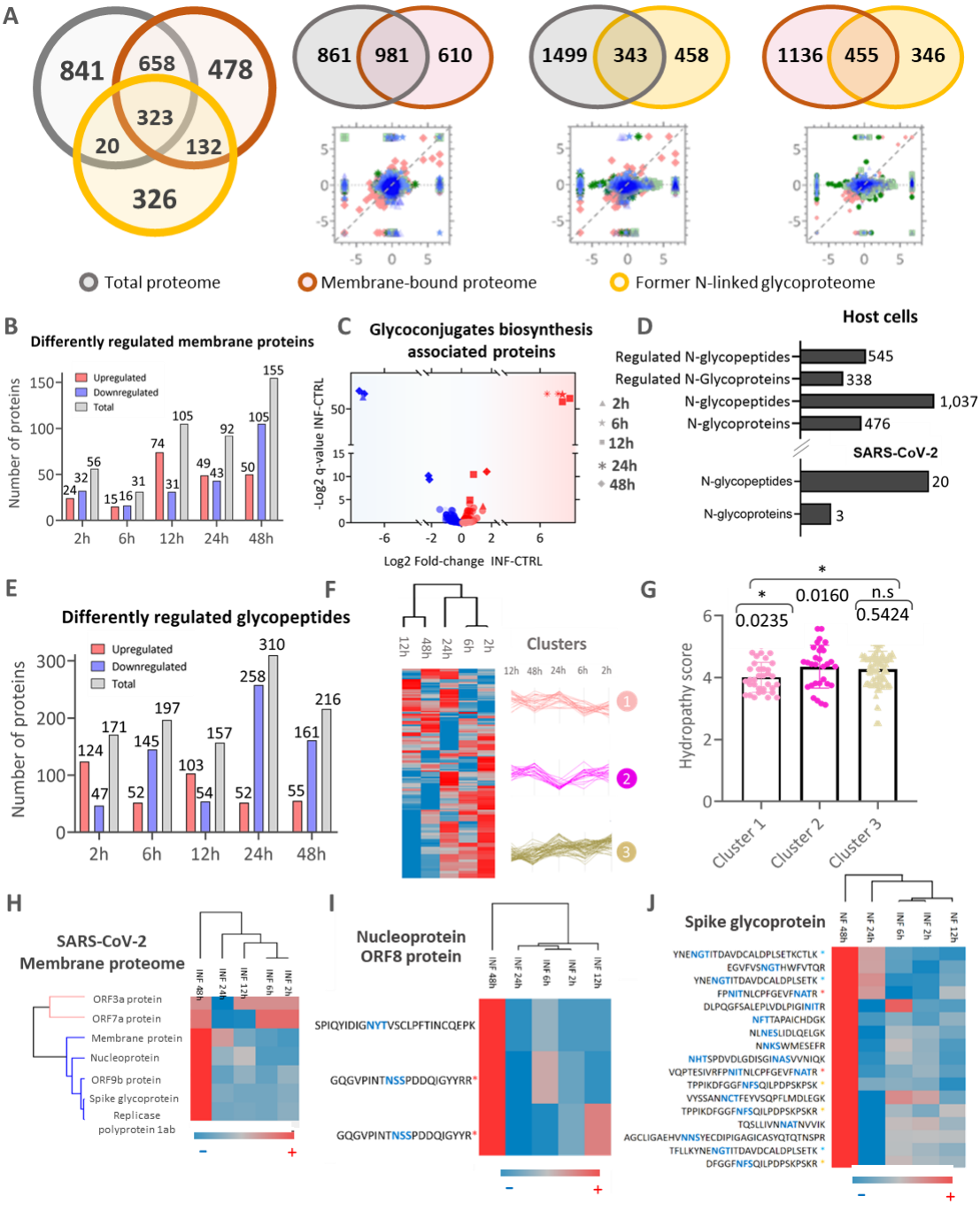

389

390 **Figure 3. Membranome and former N-linked host cells upon SARS-CoV-2 infection.**
391 Venn diagram indicating common and exclusive proteins identified in the total proteome
392 (gray), membranome (yellow), and N-deglycoproteome (orange) analysis. Scatter plots
393 indicate the correlation between common proteins between the three datasets **(A)**; Vero
394 cells proteins differentially regulated membrane proteins at 2, 6, 12, 24 and 48 hpi (q-

value <0.05). Up, down and total regulated proteins are represented in red, blue and grey bars, respectively **(B)**. Regulation of membrane proteins associated with the glycoconjugates biosynthesis according to time of infection (**C**); Glycopeptides and glycoproteins identified in the host cells and SARS-CoV-2 **(D)**; Differently regulated N-deglycopeptides between the infected (INF) and control (CTRL) groups (q-value <0.05 **(E)**; Formerly N-linked glycopeptides differentially regulated in at least one comparison between infected (INF) and control (CTRL) groups **(F)**; Hydrophobicity score of clusters of differently regulated peptides in heatmap A (**G**); SARS-CoV-2 viral proteins identified together with host membrane (**H**); SARS-CoV-2 formerly N-linked glycopeptides mapped to nucleoprotein, replicase polyprotein 1a, ORF8 glycoprotein **(I)** and spike glycoprotein **(J)**. Blue sequences present N-glycosylation sequon.

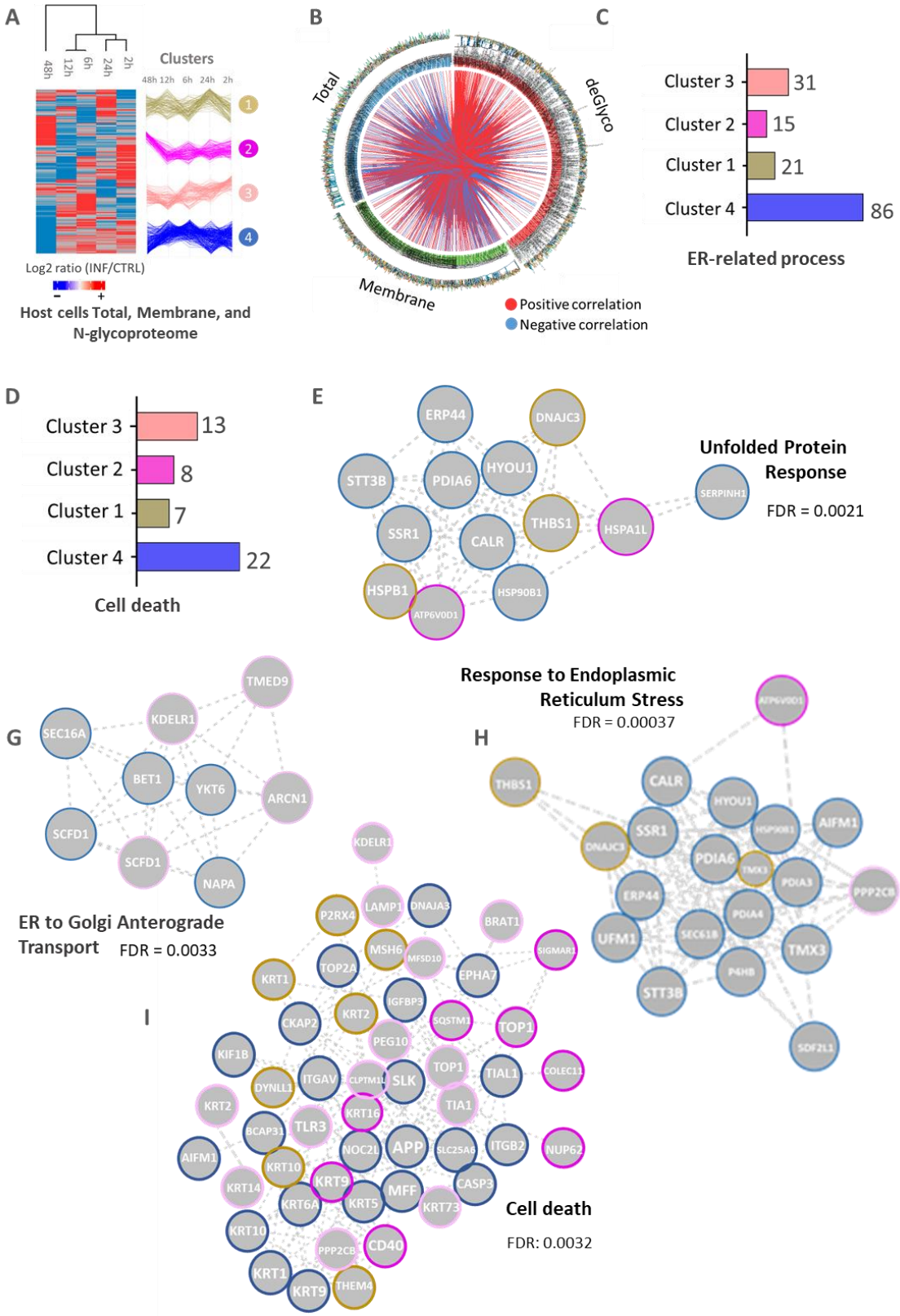

409

410 **Figure 4. Integrative analysis of MS-based proteome, membranome and N-**
411 **linked deglycoproteome**. Differentially regulated host proteins in at least one
412 group of a dataset **(A)**; Correlation map indicating the positive (red) or negative
413 (blue) correlation between regulated proteins/peptides of different experimental
414 approaches **(B)**; Proteins associated to Endoplasmic reticulum (ER) stress **(C)** and

cell death **(D)** identified in the clusters of heatmap and respective enriched protein-protein interaction networks (q-value <0.05) **(E-I)**.

To further explore and confirm the effects of the viral infection, we performed immunoblotting analysis focusing on specific molecular pathways regulated in a time-course manner. In particular, we evaluated the activation of ER-stress, unfolded protein response (UPR), cell death and oxidative stress markers. This validation was performed in Vero CCL-81 monkey and Calu-3 human cell lines. Increased phosphorylation levels of PERK and eIF2α as well as protein levels of ATF4 were observed after 2h of viral infection presenting a peak at 6h in both cell lines tested (**Figures 5A-D, Supplementary Figures 3 and 4**). These results further confirmed that this UPR pathway was activated by the virus (**Figure 5A-D, Supplementary Figures 3 and 4**). In addition, higher levels of ATF6 and phosphorylated IRE1α were seen only after 48h of infection (**Figure 5E, Supplementary Figures 3 and 4**). Interestingly, phosphorylated IRE1α was not increased in Calu-3 cells (Supplementary Figure 3). The proteomic data have also detected higher levels of proteins related to apoptosis induction. Indeed, the western blot results demonstrated that CHOP, a protein linking UPR and apoptosis activation [38], presented increased levels upon 6h of viral infection only in ~~the more susceptible~~ Vero cells, indicating that apoptosis has been triggered in these cells by the virus (**Figure 5G, Supplementary Figures 3 and 4**). The detection of higher levels of cleaved caspase-3 clearly demonstrated apoptosis activation upon 48h of viral infection (**Figure 5H**).

Additionally, we investigated PERK-NRF2 pathway axis to understand the increased antioxidant response observed in the infected cells. Higher levels of these proteins were observed after 6 and 12h of viral infection (**Figures 5F, 5H, Supplementary Figures 3 and 4**). Interestingly, the proteomic data evidenced significant decreasing levels of proteins displaying a function related to antioxidant response in Vero cells at the same time points shown in **Figure 5F** and **Supplementary Figures 3 and 4**. These data pointed at a generation of oxidative stress upon viral infection with the corresponding activation of early antioxidant response in the host cells. Viral infection has been shown to induce

oxidative stress by ROS production to facilitate their replication in the host cell [39,40]. In some cases, viruses have the ability to suppress the NRF2 pathway in their favor [41].

Since it is known that NRF2 can prevent cellular and tissue damage by decreasing the production of DAMPs (Damage-Associated Molecular Patterns) that are released by necrotic cells [42]. In addition, oxidative stress generated by redox imbalance contribute to viral pathogenesis, resulting in a massive induction of cell death [43]. Therefore, we decided to investigate some mechanisms of regulated cell death (RCD). Beside the caspase activation already described in Vero cells, we studied whether necroptosis and ferroptosis were also activated. For this purpose, the protein levels and/or the phosphorylation state of some components of these pathways were analyzed by western blot. Higher levels of MLKL phosphorylation were observed after 48h of viral infection in these cells indicating that part of cell death could be caused by necroptosis activation [44] (**Supplementary Figure 3**). This effect was not seen in Calu-3 cells. Higher levels of GPX4 at 6h of viral infection, in Vero and Calu-3 cells (**Supplementary Figure 3 and 4**), could indicate that ferroptosis was not being activated, because GPX4 may be part of the antioxidant mechanism activated by the PERK-NRF2 pathway, since GPX4 is also an established NRF2 transcriptional target [45]. Overall, these results indicate that at least two cell death regulated pathways are being activated by viral infection in Vero cells. Unlike what was observed in Vero cells, Calu-3 cells presented no changes in cleaved caspases or MLKL phosphorylation levels upon viral activation until the last time point studied. These results led us to conclude that different cells may display different kinetics in cell death signaling pathways activation. This could be related to the existence of stronger homeostatic responses being triggered to avoid cell death. Indeed, previous results from our group have shown that Calu-3 cells exposed to viral infection start show signs of cell death only after 72h (data not shown).

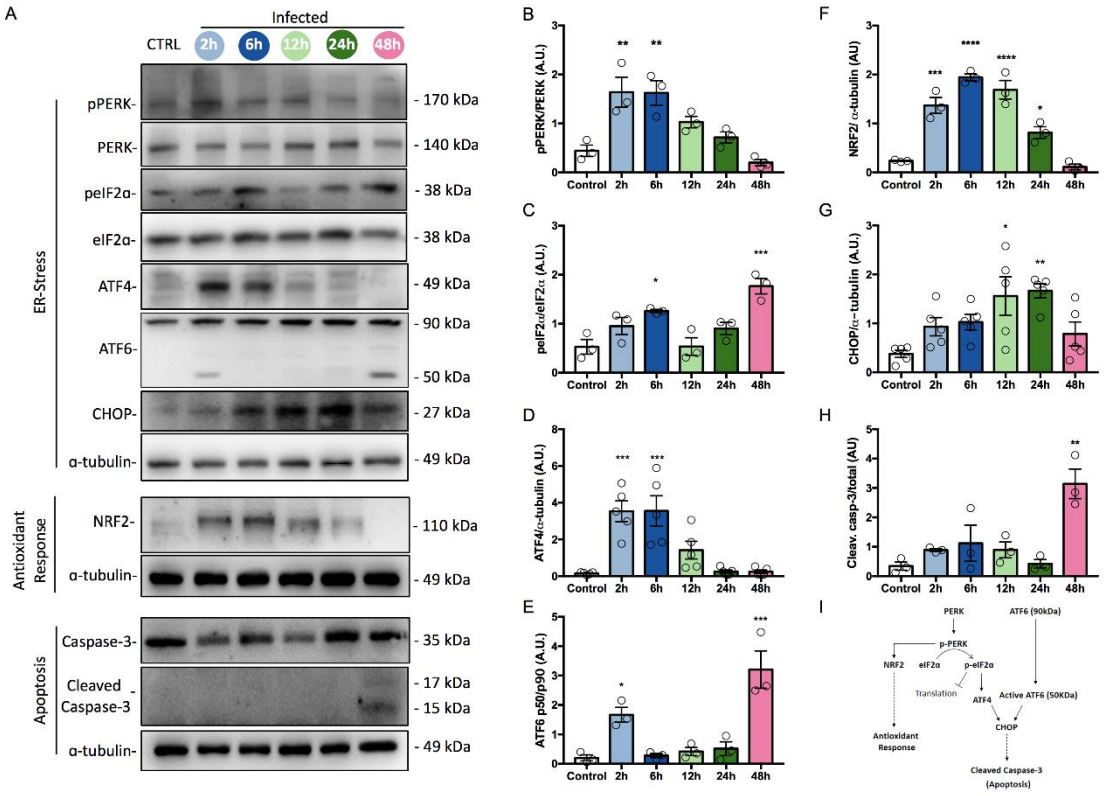

Figure 5. SARS-CoV-2 infection induces ER-stress, antioxidant response and apoptosis in Vero cells. Representative images of Western blots of ER-stress, antioxidant response and apoptosis proteins, as indicated **(A)**. The corresponding quantification of protein ratios of pPERK/PERK **(B)**, peIF2α/eIF2α **(C)**, ATF4/α-tubulin **(D)**, ATF6 p50/ ATF6 p90 **(E)**, NRF2/α-tubulin **(F)**, CHOP/α-tubulin **(G)** and Cleaved Caspase-3/Caspase-3 **(H)**. Schematic representation of ER-stress, antioxidant response and apoptosis pathways activated after SARS-CoV-2 infection **(I)**. Each dot represents an independent experiment (n≥3 independent experiments; **** p<0.0001; *** p<0.001; ** p<0.005; *p<0.05 vs Control).

To access further translational aspects of our *in vitro* findings, we re-analyzed transcriptome data obtained from lung autopsies of eight patients who died as a result of COVID-19 (**Figure 6A**) and the respective controls [37]. Using a dedicated pipeline to reprocess the data with higher stringency in the statistical test, we identified 1,398 regulated transcripts, being 636 up-regulated and 762 down-regulated (**Figure 6B**). PCA analysis showed diverse transcriptome profile between COVID-19 patients and controls. (**Figure 6C**). We observed that differentially regulated transcripts were involved in several processes linked to

ER stress, such as cell death, chaperone-mediated folding, 'de novo' protein folding, protein localization to ER, programmed cell death, and protein folding, confirming the proteomic data (**Figures 6G and H**). Mapping ER-stress transcripts and proteins in clinical specimens from patients infected with SARS-CoV-2, it was possible to identify that RCN3, UCHL1, and ERO1A are upregulated in the lung at the level of transcript and proteome [37]. Moreover, we found 51 up-regulated and 45 down-regulated confirming the alteration of the host glycosylation biosynthetic machinery upon SARS-CoV-2 infection (**Figure 6F)**. Interestingly, hierarchal clustering analysis showed that the infected samples 1, 3, and 4 had a distinguished pattern of up-regulated ER-related transcripts (**Figure 6D**). It is worth to mention that the average survival time after being hospitalized was significantly higher in these three patients compared to the others (**Figure 6E**). These data confirm the regulation of ER-stress proteins during SARS-CoV-2 infection.

Taken together, our data indicated that SARS-CoV-2 infection modulates glycoconjugates biosynthetic machinery changing the host global protein glycosylation profile. Additionally, ER stress induced in infected cells activates PERK-eIF2α-ATF4-CHOP UPR pathway finally leading to apoptosis induction. Cell death might also occur by necroptosis, linked to antioxidant response and activation of PERK-NRF2 pathway and MLKL phosphorylation. These *in vitro* phenomena were also observed in human lung biopsies of COVID-19 patients, indicating a role of ER protein modulation and survival time.

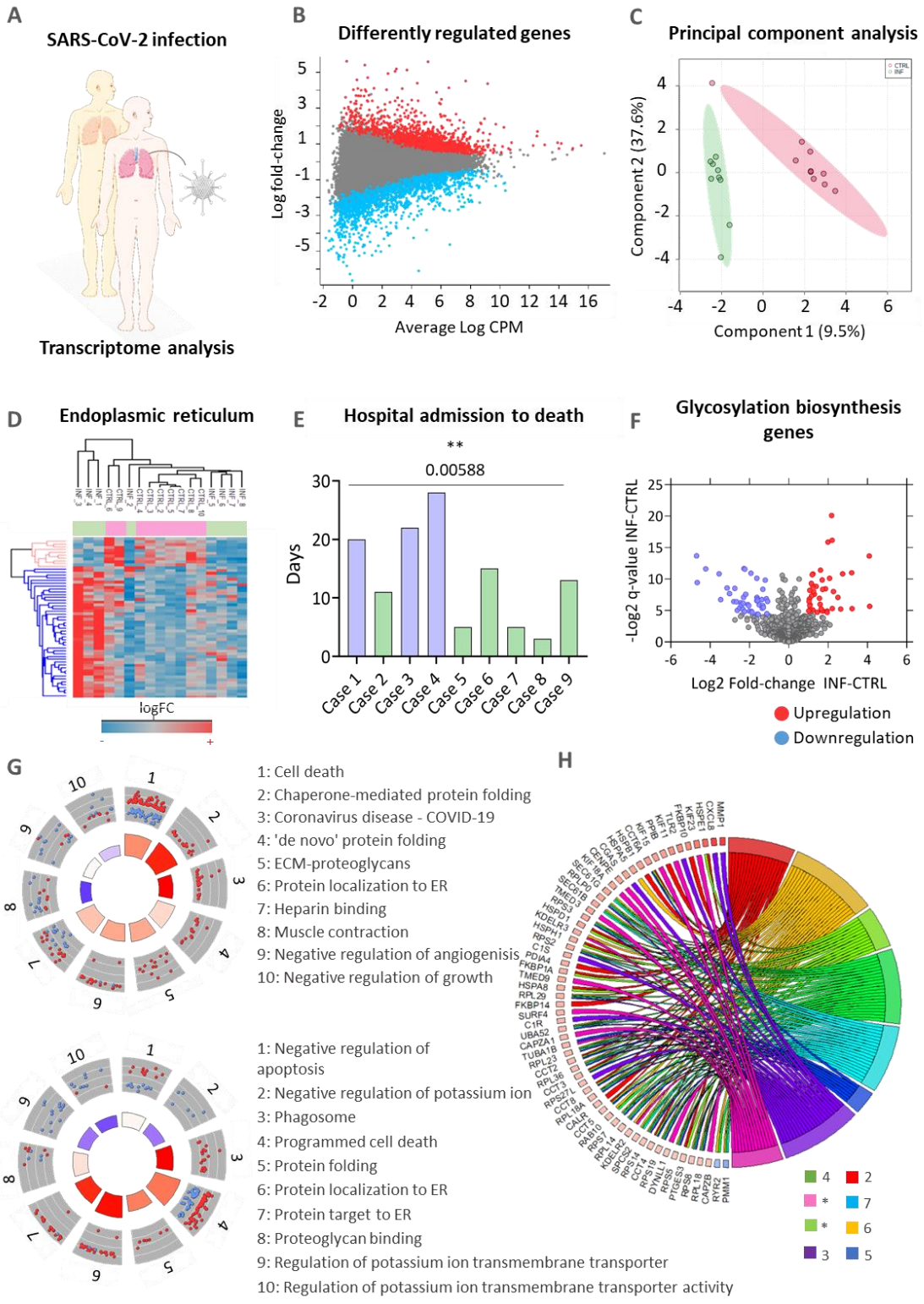

520

521 **Figure 6**. RNA-seq reanalysis data including samples of the lung of patients
522 infected with SARS-CoV-2 and healthy samples from cancer donors (A),
523 indicating the Differently regulated genes (B); Principal component analysis (C);
524 Heatmap for differently regulated genes that are located in the endoplasmic
525 reticulum (ER) (D); Hospital admission to death in days (E); Genes associated with
526 the glycosylation biosynthesis alteration (F) and Gene ontology analysis (G-J).

The (*) corresponds to Golgi-to-ER retrograde transport and the Establishment of protein localization to endoplasmic reticulum pathways.

DISCUSSION

SARS-CoV-2 hijacks several host machineries to control immune reaction [46], viral protein translation [47], viral genome packing into nascent viral particles as well as support the release of mature virus particles. Host cellular machineries are redirected to synthesize and remodel viral proteins through post-translational modifications such as proteolytic cleavages, disulfide bridges formation, phosphorylation, ubiquitination and glycosylation [48–53]. Thus, in this study we sought out which processes and pathways could be changed by the viral infection. Our proteomics approach yielded a total of 2778 proteins being 1842, 1591 and 801 proteins identified in the total, membrane and glycosylated proteome, respectively. Even if the number of total identified proteins is comparable to other studies using similar technological platforms, we analyzed different time-points, cell lines and MOI. Grenga et al. (2020) identified 3220 host proteins and 6 SARS-CoV-2 proteins over 5 time-points evaluated (1, 2, 3, 4 and 7 days) and two MOI (0.1 and 0.001) [54]. Stukalov et al. (2021) identified a total of 5862 proteins in ACE2-expressing A549 cells infected with SARS-CoV-2 and SARS-CoV over three time points (6, 12, 24 hpi); concerning only regulated proteins, they found a total of 272 [48], while we identified 443 regulated proteins using only Vero cells infected with SARS-CoV-2 over five time points. It should be noted that we used an earlier (2 h) and later (48 h) time point that influence the number of regulated proteins. Bojkova et al. (2020) identified over 7,000 proteins using Caco-2 infected cells at four time-points (2, 6, 10 and 24 hours) being over 3,400 regulated proteins [55]. Using two different MOI (0.1 and 3), Zecha et al. (2020) identified 7,287 proteins and approximately 1,500 regulated host proteins in SARS-CoV-2 infected Vero cells in a single time-point (24 hpi) [56].

Our results pointed at host proteome remodeling upon viral infection, consisting of protein global downregulation in all evaluated time points, except at 6 and 48 hpi. Such pattern was also recently reported in the total proteome analysis

558 performed by Stukalov and collaborators (2021). Although they did not analyze
559 the proteomic profile at 48 hpi, they observed that proteins were mostly down-
560 regulated at 12 and 24 hpi but being up-regulated at 6 hpi [48]. Since it has already
561 been shown that viral replication starts at 6 hpi [57,58], the observed global protein
562 up-regulation at 6 hpi could imply an initial response from the cell, followed by
563 protein inhibition due to viral influence until 48 hpi, when cell death events are
564 most prevalent. This remodeling was supported by PCA analysis, which showed
565 a clear time-dependent separation.

566 Among the identified proteins, we found 8 viral proteins in all time-points.
567 Compared with the work in Caco-2 cells performed by Bojkova et al. (2020) [58], we
568 did not identify the non-structural protein 8, and instead of identifying the
569 replicase polyprotein a, we have identified the replicase polyprotein 1ab. Our data
570 have confirmed part of the data published by Davidson et al. [59]using Vero cells.
571 Indeed, we have identified the non-structural protein 9b but not proteins 8 or 9a.
572 The viral proteins N, S, M, ORF1ab, ORF3a and ORF7a identified in this study
573 were also found in the recent work of Grenga and collaborators (2020) [54].

574 Regarding regulated biological processes and pathways, our results showed
575 similarities when compared to other proteomics studies. A cluster analysis of
576 SARS-CoV-2 infected Vero cells over a period of seven days indicated that
577 membrane trafficking, protein pre-processing in the ER, clathrin-mediated
578 endocytosis, vesicle-mediated transport, and viral life cycle were enriched during
579 the infection [54]. Similarly, we have reported membrane trafficking, pathways
580 related to the viral life cycle, and post-translational protein modification enriched
581 in the regulated protein dataset. As already shown in infected Caco-2 cells, our
582 pathway analysis has also identified that upon viral infection, TCA and respiratory
583 electron transport as well as the carbohydrates metabolism processes were
584 modulated. Other common regulated processes observed in the literature are
585 autophagy, IFN-α/β induction or signaling, cell adhesion, and extracellular matrix
586 organization [48,56], being the regulation of IFN-α/β pathway extensively explored as
587 a drug target for viral replication inhibition [48]. Besides similar processes and
588 pathways during SARS-CoV-2 infection, we have focused on the effects of viral

589 replication in the ER-stress and UPR in a time-dependent manner. Through
590 hierarchical clusters, we identified 3 main clusters that showed the effects of the
591 viral infection in a time-dependent manner. Among the biological processes
592 identified in the clusters, asparagine N-linked protein glycosylation, response to
593 stress, unfolded protein response and post-translational protein modification
594 were increased in the intermediate time-points, but decreased at 48 hpi.

595 Glycosylation of viral proteins is an important process that regulates viral
596 assembly and infectivity. The structural and functional role of glycosylation in the
597 SARS-CoV-2 spike protein has been widely investigated [52,60–66]. Of note is the fact
598 that 35% of the SARS-CoV-2 spike glycoprotein contains carbohydrate moieties,
599 which have profound influence on the viral infectivity, susceptibility to antibody
600 neutralization [67,68]. The N-linked glycosylation sites of spike proteins have been
601 related to alterations in its open or closed state thus interfering in its capacity to
602 bind to the receptor [69]. We found 17 formerly N-glycopeptides and 14
603 glycosylation sites in the Spike glycoprotein. There are 22 potential glycosylation
604 sites in the SARS-CoV-2 Spike protein and the number of reported occupied sites
605 range between 17 and 22 [51,63,70,71]. The processing of the spike glycoprotein
606 through the ER and Golgi compartments represents an important step in
607 controlling the virion assembly and inhibition of the N- and O-glycan maturation,
608 which has been shown to interfere with virulence [70,72–75]. Additionally, we mapped
609 the N-linked glycosylation site of ORF8 protein of SARS-CoV-2. This accessory
610 protein has less than 20% identity with the same protein in SARS-CoV,
611 highlighting divergencies between the two viruses [76]. Although this protein does
612 not appear to be essential for viral replication, it has been shown to disrupt IFN-I
613 and promote MHC-I downregulation [77,78]. ORF8 contains a signal peptide for ER
614 import and interacts with several proteins within the ER. In this study, we have
615 mapped one N-linked glycosylation site at N78. This site is close to a SARS-CoV-
616 2-specific sequence YIDI[76], that has been reported to be involved in noncovalent
617 dimerization [36]. Antibodies against ORF8 were identified as serological markers
618 of acute, convalescent and long-term response to SARS-CoV-2 infection [79].
619 Therefore, it would be relevant to evaluate the role of site-specific ORF8
620 glycosylation in antibody neutralization.

The fact that asparagine N-linked glycosylation was enriched in the biological processes regulated during viral infection may indicate that the continuous translation of viral glycoproteins is overwhelming the glycosylation machinery capacity, increasing the number of proteins with aberrant glycosylation. This dysregulated process could contribute with ER stress, since it can increase protein misfolding [80,81]. Proteins related to asparagine N-linked glycosylation were reported among the top 10% of proteins following viral gene expression [58]. Thus, indicating a metabolic challenge for the host glycosylation machinery promoted by viral infection. A recent study has demonstrated that N-glycosylation inhibitors were able to reduce SARS-CoV-2 infection in Vero and HEK293^{ACE-2} cells. Moreover, genetic ablation of this pathway using siRNAs and virions presenting N-glycosylation defects also reduced the infection rate [82]. Since we found that five enzymes involved in the glycosylation biosynthesis (CHST12, CHST14, B4GALT3, GCNT1 and MGAT2) were mainly up-regulated in the intermediate time-points, but down-regulated at 48 hpi, our data showed a complete remodeling of the N-linked protein glycosylation process. Recently, the downregulation of this process was also evaluated by the targeting of 88 host glycogenes by siRNAs in a study on the secretion of hepatitis B surface antigen (HBsAg) and HBV DNA, which showed that targeting CHST12 reduced the HBV DNA levels by >40% in EPG2.2.15.7 cells [83]. This further support the hypothesis that viral the viral infection can modulate the host glycosylation machinery.

Aberrant glycosylation can interfere in protein folding (PMID: 24609034). The effects of viral infection on protein folding were also observed in the functional enrichment analysis of the differentially abundant proteins identified in this study. Indeed, at 6 hpi we observed an increase in ER stress caused by misfolded or unfolded proteins with the up-regulation of UPR. Moreover, we confirmed the activation of ER stress and UPR in SARS-CoV-2-infected Vero and Calu-3 cells using western blotting. Several evidences suggest that ER stress and UPR activation are the main contributors to the pathogenesis of various diseases including viral infections [84]. Recent SARS-CoV-2 host interactome has been performed in HEK293, human bronchial epithelial 16HBEo− and A549 cells [6,48,85]. Proteins related to ER stress such as thrombospondin-1, GRP78, DJB11,

653 calnexin and F-box only protein 2 were found to interact with the spike protein
654 [86,87]. In addition, other SARS-Cov-2 proteins were found to interact with proteins
655 involved in ER protein quality control, ER morphology and protein glycosylation [6].
656 Cell surface GRP78 was identified to interact with the Middle East respiratory
657 syndrome coronavirus spike glycoprotein and increase the viral entry [88].
658 Furthermore, SARS-CoV S glycoprotein was found to bind calnexin and increase
659 its infectivity by modulating the maturation of the glycans [89]. Another host-virus
660 protein-protein interaction analysis also pointed ER stress as being one of the
661 pathways most affected by the SARS-CoV-2 proteins [90]. SARS-CoV 3a protein
662 has been shown to be able to induce ER stress by activating PERK pathway
663 resulting in increasing levels of eIF2α phosphorylation and ATF4 protein level,
664 which finally promoted the synthesis of CHOP and increased Huh7 cells apoptosis
665 [91]. It is important to note that the authors have not observed signs of ATF6
666 signaling pathway activation [91]. Another study with SARS-CoV showed that the
667 suppression of the spike protein inhibits the up-regulation of BiP and GRP94
668 chaperones, which are targets of PERK-eIF2α-ATF4 pathway activation.
669 Moreover, the authors reported the inhibition of this pathway promoted a
670 decrease of these chaperones, pointing once again that UPR modulation by the
671 virus could facilitate the infection process [92]. The stress-responsive heat shock
672 protein gene HSP90AA1 was reported to be induced in H1299 and Calu-3 cells
673 during infection, adding more evidence of ER stress occurring upon SARS-CoV-
674 2 replication [93]. The activation of CHOP due to stress can induce the expression
675 of BIM, linking ER stress induction with apoptosis activation [94]. Moreover, ATF4
676 and CHOP can also activate the translation of genes related to translational
677 components which will enhance protein synthesis in the cell, causing an increase
678 in ROS production and consequently cell death [95].

679 It has been shown prolonged ER stress can activate apoptosis pathway, which
680 will conclude with the assembly of the apoptosome and caspase-3 activation [96].
681 We observed that apoptotic-related processes were mainly modulated in the late
682 time events, indicating that cell death may be more frequent at 48 hpi.
683 Additionally, the enriched pathway analysis showed that these processes started

684 at 12 hpi and remained active at 24 hpi. Although ER stress is predominantly the
685 main cause of stress observed in this study, viruses have been shown to induce
686 oxidative stress by ROS production in to facilitate their replication in the host cell
687 [39,40]. Viral infections can induce the release of pro-oxidant cytokines such as the
688 tumor necrosis factor (TNF), which lately will produce the hydroxyl radical OH [97].
689 A study in Huh-7 cells indicated that Ca^{2+} released from the ER as a consequence
690 of the human hepatitis C virus-induced ER stress will lead to an increase Ca^{2+}
691 upload by the mitochondria, where it will promote the generation of higher ROS
692 levels and the consequent increase in oxidative stress [98–101].

693 Besides caspase activation, we found increased phosphorylation of MLKL at 48
694 hpi indicating a possible contribution of necroptosis induction upon viral infection.
695 This dual mode of cell death mechanism has been reported in infected HFH4-
696 hACE2 transgenic mouse model, Calu-3 cells and in postmortem lung sections of
697 fatal COVID-19 patients [102].

698 Since our study clearly points towards protein folding, ER stress and UPR
699 modulation, which lead to cell death in later events, we sought if the effects of
700 viral infection in these processes could also be seen not only *in vitro* models but
701 also in human tissue biopsies. Our re-analysis of the post-mortem lung
702 transcriptome of COVID-19 patients showed that processes related to protein
703 folding and cell death are being regulated, which are in accordance with
704 proteomics analysis showing increased levels of ER stress and UPR modulation.
705 The processes identified in our re-analysis were not explored by the authors of
706 the original work as their results focused on neutrophil activation and neutrophil-
707 mediated immunity, extracellular traps and extracellular structure organization [37].
708 Interestingly, ER stress related pathways and processes are not well explored in
709 transcriptomic studies, being processes and pathways related to immune
710 response and inflammation more commonly found in the literature, such as
711 modulation of cytokine-mediated signaling pathway, interferon signaling, TNF-
712 signaling, and interleukin-mediated signaling [54,103–105]. Nevertheless, the
713 enrichment analysis of these works often contains processes and pathways
714 related to proteins transport and localization to ER. For example, the

715 transcriptional response of hACE2 receptor-transduced A549 and Calu-3 cell
716 lines to SARS-CoV-2, MERS-CoV, or influenza A virus (IAV) infections focused on
717 the autophagy pathway and mitochondrial processes, but UPR modulation was
718 observed in the A549 lung epithelial cell line [106]. Interestingly, the authors
719 compared the A549 cells infected with SARS-CoV-2 and IAV and found UPR
720 modulated only in SARS-CoV-2 infection [106]. A recent study has shown that
721 recombinant expression of SARS-CoV-2 spike protein in HEK293T cells induces
722 ER-stress and UPR activation [107]. The increased expression of GRP78 and
723 phosphorylated eIF2α was reported together with increased LC3 II at 24 hours
724 post spike transfection [107]. Treatment of transfected cells with UPR modulators
725 reduced the ER stress levels [107]. However, this study did not provide a kinetic and
726 comprehensive measurement of ER-stress and UPR activation, as reported here.

727 Our results corroborate recent findings on the identification of serum ER stress
728 markers (GRP78 and phosphorylated PERK) in the lungs of COVID-19 patients
729 with severe complications [108]. Proteomic analysis of multiple organs from patients
730 infected with SARS-CoV-2 showed that, in addition to the lungs, there is an
731 increase in ER stress in the renal cortex and liver cells. RCN3 is a protein located
732 in the ER lumen that acts in the remodeling during lung injury [109]. RCN3-deficient
733 mice has been shown to result in increased ER stress and apoptosis [109,110]. The
734 ERO1A protein is a CHOP-activated oxidase that promotes ER hyperoxidization
735 and affects the activation of CHOP-dependent apoptosis by stimulating the IP3R1
736 1,4,5-triphosphate inositol receptor [111,112]. The UCHL1 protein performs important
737 functions related to protein degradation [113]. In addition, it was observed that
738 UCHL1 levels influence cell homeostasis under normal conditions of growth and
739 oxidative stress [114]. The transcriptome of silenced cells for UCHL1 showed
740 downregulation of genes associated with proteasome activity and upregulation of
741 genes linked to ER-stress [115]. Moreover, we observed that samples from COVID-
742 19 patients with higher expression of ER transcripts were associated to longer
743 survival period.

744 Taken together, this study provides a time-resolved and large-scale
745 characterization of the total, membrane and glycoproteome of SARS-CoV-2-

746 infected Vero CCL-81 cells. The modulation of specific processes including viral
747 and host protein glycosylation, ER-stress and UPR were validated using western
748 blotting and reanalysis of transcriptomic data of human clinical specimens. These
749 data highlight the importance of ER-stress and UPR modulation as a host
750 regulatory mechanism during viral infection and could point to novel therapeutic
751 targets.

752 **Acknowledgments:**

753 The work was supported by grants and fellowships from FAPESP (2018/18257-1,
754 2018/15549-1, 2020/04923-0 to GP; 2016/04676-7 to AFS; 2019/09517-2 to
755 GSA; 2017/24769-2 to RRGM; 2016/20045-7 and 2020/06409-1 to ELD), from
756 Coordenação de Aperfeiçoamento de Pessoal de Nível Superior – Brasil (CAPES)
757 (Código de Financiamento 001 to LR-F; 88887.131387/2016-00 to DBA) and from
758 Conselho Nacional de Desenvolvimento Científico Tecnológico (CNPq) ("bolsa
759 de produtividade" to GP).

760 Professor Suely Kazue Nagahashi Marie from FM-USP is acknowledged for
761 advice during manuscript writing and all the support.

762 **Author Contributions**

763 GP conceived the idea. LR-F and GP designed the experiments. LR-F, LCL, CBA
764 and GP prepared the samples for proteomics analysis. LR-F, LCL, JMdS and GP
765 analyzed the mass spectrometry data, performed bioinformatic analyses and
766 wrote the manuscript. RRGM, DBA, DBLO and ELD performed the viral infection
767 and RT-qPCR. CW and CRFM assisted on data interpretation. VdMG, AFS, GSA
768 and LL performed and analyzed the western blotting. All authors contributed in
769 editing the manuscript and approved the final version.

770 **References**

771 1. Guan, W. et al. Clinical Characteristics of Coronavirus Disease 2019 in China. 1–
772 13 (2020) doi:10.1056/NEJMoa2002032.
773 2. Zhang, L. & Liu, Y. Potential interventions for novel coronavirus in China: A
774 systematic review. J. Med. Virol. 92, 479–490 (2020).
775 3. Sohrabi, C. et al. World Health Organization declares global emergency: A review
776 of the 2019 novel coronavirus (COVID-19). Int. J. Surg. 76, 71–76 (2020).

4. Chen, Y. & Li, L. SARS-CoV-2: virus dynamics and host response. Lancet Infect. Dis. 20, 515–516 (2020).
5. Mathews, P. et al. Host-pathogen interaction in COVID-19: Pathogenesis, potential therapeutics and vaccination strategies. Immunobiology 225, (2020).
6. Gordon, D. E. et al. A SARS-CoV-2 protein interaction map reveals targets for drug repurposing. Nature 583, 459–468 (2020).
7. Gordon, D. E. et al. Comparative host-coronavirus protein interaction networks reveal pan-viral disease mechanisms. Science (80-.). 370, (2020).
8. Lum, K. K. & Cristea, I. M. Proteomic approaches to uncovering virus-host protein interactions during the progression of viral infection. Expert Rev. Proteomics 13, 325–340 (2016).
9. Rudd, P. M. et al. Glycosylation and the Immune System. Science (80-.). 2370, (2012).
10. Reitter, Jullie N; Means, Robert E; Desrosiers, R. C. A role for carbohydrates in immune evasion in AIDS. Nat. Med. 56, 679–684 (1998).
11. Wagner, R., Wolff, T., Herwig, A., Pleschka, S. & Liebig-universita, J. Interdependence of Hemagglutinin Glycosylation and Neuraminidase as Regulators of Influenza Virus Growth : a Study by Reverse Genetics. J. Virol. 74, 6316–6323 (2000).
12. Shirato, K. et al. Viral envelope protein glycosylation is a molecular determinant of the neuroinvasiveness of the New York strain of West Nile virus. J. Gen. Virol. 85, 3637–3645 (2004).
13. Laine, R. A. The case for re-examining glycosylation inhibitors, mimetics, primers and glycosylation decoys as antivirals and anti-inflammatories in covid19. Glycobiology 30, 763–767 (2020).
14. Dwek, R. A., Butters, T. D., Platt, F. M. & Zitzmann, N. Targeting glycosylation as a therapeutic approach. Nat. Rev. Drug Discov. 1, 65–75 (2002).
15. Fung, T. S. & Liu, D. X. Coronavirus infection, ER stress, apoptosis and innate immunity. Front. Microbiol. 5, 1–13 (2014).
16. Ron, D. & Walter, P. Signal integration in the endoplasmic reticulum unfolded protein response. Nat. Rev. Mol. Cell Biol. 8, 519–529 (2007).
17. Cao, S. S. & Kaufman, R. J. Unfolded protein response. Curr. Biol. 22, R622–R626 (2012).
18. Greco, T. M. & Cristea, I. M. Proteomics Tracing the Footsteps of Infectious Disease *. Am. Soc. Biochem. Mol. Biol. 5–14 (2017) doi:10.1074/mcp.O116.066001.
19. Weekes, M. P. et al. Quantitative Temporal Viromics : An Approach to Investigate Host-Pathogen Interaction. Cell 157, 1460–1472 (2014).
20. Araujo, D. B. et al. SARS-CoV-2 isolation from the first reported patients in brazil and establishment of a coordinated task network. Mem. Inst. Oswaldo Cruz 115, 1–8 (2020).
21. Corman, V. et al. Detection of 2019 novel coronavirus (2019-nCoV) by real time RT-PCR. Euro Surveill 25, 1–8 (2020).
22. Rosa-Fernandes, L. et al. Cellular Imprinting Proteomics Assay: A Novel Method for Detection of Neural and Ocular Disorders Applied to Congenital Zika Virus Syndrome. J. Proteome Res. 19, 4496–4515 (2020).
23. Palmisano, G. et al. A novel method for the simultaneous enrichment, identification, and quantification of phosphopeptides and sialylated glycopeptides applied to a temporal profile of mouse brain development. Mol. Cell. Proteomics 11, 1191–1202 (2012).
24. Fujiki, Y., Hubbard, L., Fowler, S. & Lazarow, P. B. Isolation of intracellular membranes by means of sodium carbonate treatment: Application to Endoplasmic Reticulum. J. Cell Biol. 93, 97–102 (1982).

828 25. Palmisano, G. et al. Selective enrichment of sialic acid-containing glycopeptides
829 using titanium dioxide chromatography with analysis by HILIC and mass spectrometry.
830 Nat. Protoc. 5, 1974–1982 (2010).
831 26. Kawahara, R. et al. Integrated proteomics reveals apoptosis-related mechanisms
832 associated with placental malaria. Mol. Cell. Proteomics 18, 182–199 (2019).
833 27. Mysling, S., Palmisano, G., Hojrup, P. & Thaysen-Andersen, M. Utilizing ion-
834 pairing hydrophilic interaction chromatography solid phase extraction for efficient
835 glycopeptide enrichment in glycoproteomics. Anal. Chem. 82, 5598–5609 (2010).
836 28. Perez-Riverol, Y. et al. The PRIDE database and related tools and resources in
837 2019: Improving support for quantification data. Nucleic Acids Res. 47, D442–D450
838 (2019).
839 29. Mart, P. et al. General Statistical Framework for Quantitative Proteomics by Stable
840 Isotope Labeling. J. Proteome Res. 13, 1234–1247 (2014).
841 30. Walter, W., Sánchez-Cabo, F. & Ricote, M. GOplot: An R package for visually
842 combining expression data with functional analysis. Bioinformatics 31, 2912–2914
843 (2015).
844 31. Reimand, J., Kull, M., Peterson, H., Hansen, J. & Vilo, J. G:Profiler-a web-based
845 toolset for functional profiling of gene lists from large-scale experiments. Nucleic Acids
846 Res. 35, 193–200 (2007).
847 32. Jassal, B. et al. The reactome pathway knowledgebase. Nucleic Acids Res. 48,
848 D498–D503 (2020).
849 33. Osorio, D., Rondón-Villarreal, P. & Torres, R. Peptides: A package for data mining
850 of antimicrobial peptides. R J. 7, 4–14 (2015).
851 34. Rohart, F., Gautier, B., Singh, A. & Lê Cao, K. A. mixOmics: an R package for
852 'omics feature selection and multiple data integration. bioRxiv 1–19 (2017)
853 doi:10.1101/108597.
854 35. Wrapp, D. et al. Cryo-EM structure of the 2019-nCoV spike in the prefusion
855 conformation. bioRxiv 1263, 1260–1263 (2020).
856 36. Flower, T. G. et al. Structure of SARS-CoV-2 ORF8, a rapidly evolving coronavirus
857 protein implicated in immune evasion. bioRxiv 1–6 (2020)
858 doi:10.1101/2020.08.27.270637.
859 37. Wu, M. et al. Transcriptional and proteomic insights into the host response in fatal
860 COVID-19 cases. Proc. Natl. Acad. Sci. U. S. A. 117, 28336–28343 (2020).
861 38. Hu, H., Tian, M., Ding, C. & Yu, S. The C/EBP homologous protein (CHOP)
862 transcription factor functions in endoplasmic reticulum stress-induced apoptosis and
863 microbial infection. Front. Immunol. 10, 1–13 (2019).
864 39. Liu, T. et al. Reactive oxygen species mediate virus-induced STAT activation: Role
865 of tyrosine phosphatases. J. Biol. Chem. 279, 2461–2469 (2004).
866 40. Lee, Y. H. et al. Influenza A virus induction of oxidative stress and MMP-9 is
867 associated with severe lung pathology in a mouse model. Virus Res. 178, 411–422
868 (2013).
869 41. Hosakote, Y. M. et al. Viral-mediated inhibition of antioxidant enzymes contributes
870 to the pathogenesis of severe respiratory syncytial virus bronchiolitis. Am. J. Respir. Crit.
871 Care Med. 183, 1550–1560 (2011).
872 42. Tang, W., Jiang, Y. F., Ponnusamy, M. & Diallo, M. Role of Nrf2 in chronic liver
873 disease. World J. Gastroenterol. 20, 13079–13087 (2014).
874 43. Garofalo, R. P., Kolli, D. & Casola, A. Respiratory syncytial virus infection:
875 Mechanisms of redox control and novel therapeutic opportunities. Antioxidants Redox
876 Signal. 18, 186–217 (2013).
877 44. Wang, H. et al. Mixed Lineage Kinase Domain-like Protein MLKL Causes Necrotic
878 Membrane Disruption upon Phosphorylation by RIP3. Mol. Cell 54, 133–146 (2014).

879 45. Dodson, M., Castro-Portuguez, R. & Zhang, D. D. NRF2 plays a critical role in
880 mitigating lipid peroxidation and ferroptosis. Redox Biol. 23, 101107 (2019).
881 46. Jiang, H. wei et al. SARS-CoV-2 Orf9b suppresses type I interferon responses by
882 targeting TOM70. Cell. Mol. Immunol. 17, 998–1000 (2020).
883 47. Schubert, K. et al. SARS-CoV-2 Nsp1 binds the ribosomal mRNA channel to
884 inhibit translation. Nat. Struct. Mol. Biol. 27, 959–966 (2020).
885 48. Stukalov, A. et al. Multi-level proteomics reveals host-perturbation strategies of
886 SARS-CoV-2 and SARS-CoV. bioRxiv (2020) doi:10.1101/2020.06.17.156455.
887 49. Coutard, B. et al. The spike glycoprotein of the new coronavirus 2019-nCoV
888 contains a furin-like cleavage site absent in CoV of the same clade. Antiviral Res. 176,
889 104742 (2020).
890 50. Bangaru, S. et al. Structural analysis of full-length SARS-CoV-2 spike protein from
891 an advanced vaccine candidate. bioRxiv 1094, 1089–1094 (2020).
892 51. Watanabe, Y., Allen, J. D., Wrapp, D., McLellan, J. S. & Crispin, M. Site-specific
893 glycan analysis of the SARS-CoV-2 spike. Science (80-.). 369, 330–333 (2020).
894 52. Zhang, S. et al. Analysis of glycosylation and disulfide bonding of wild-type SARS-
895 CoV-2 spike glycoprotein. bioRxiv (2021).
896 53. Roberts, D. S. et al. Structural O-Glycoform Heterogeneity of the SARS-CoV-2
897 Spike Protein Receptor-Binding Domain Revealed by Native Top-Down Mass
898 Spectrometry. bioRxiv 2021.02.28.433291 (2021).
899 54. Grenga, L. et al. Shotgun proteomics analysis of SARS-CoV-2-infected cells and
900 how it can optimize whole viral particle antigen production for vaccines. Emerg. Microbes
901 Infect. 1–18 (2020) doi:10.1080/22221751.2020.1791737.
902 55. Bojkova, D. et al. SARS-CoV-2 infected host cell proteomics reveal potential
903 therapy targets. 1–24 (2020) doi:10.21203/rs.3.rs-17218/v1.
904 56. Zecha, J. et al. Data, Reagents, Assays and Merits of Proteomics for SARS-CoV-
905 2 Research and Testing. Mol. Cell. Proteomics 19, 1503–1522 (2020).
906 57. van den Berg, D. F. & te Velde, A. A. Severe COVID-19: NLRP3 Inflammasome
907 Dysregulated. Front. Immunol. 11, 1–6 (2020).
908 58. Bojkova, D. et al. Proteomics of SARS-CoV-2-infected host cells reveals therapy
909 targets. Nature 583, 469–472 (2020).
910 59. Davidson, A. D. et al. Characterisation of the transcriptome andproteome of
911 SARS-CoV-2 reveals a cellpassage induced in-frame deletion of thefurin-like cleavage
912 site from the spikeglycoprotein. bioRxiv 1–15 (2020) doi:10.1101/2020.03.22.002204.
913 60. Miller, L. M. et al. Heterogeneity of Glycan Processing on Trimeric SARS-CoV-2
914 Spike Protein Revealed by Charge Detection Mass Spectrometry. J. Am. Chem. Soc.
915 (2021) doi:10.1021/jacs.1c00353.
916 61. Bagdonaite, I. et al. Site-Specific O-Glycosylation Analysis of SARS-CoV-2 Spike
917 Protein Produced in Insect and Human Cells. Viruses 13, 1–14 (2021).
918 62. Zhang, Y. et al. Site-specific N-glycosylation Characterization of Recombinant
919 SARS-CoV-2 Spike Proteins. Mol. Cell. Proteomics 20, 100058 (2021).
920 63. Wang, D. et al. Comprehensive Analysis of the Glycan Complement of SARS-
921 CoV-2 Spike Proteins Using Signature Ions-Triggered Electron-Transfer/Higher-Energy
922 Collisional Dissociation (EThcD) Mass Spectrometry. Anal. Chem. 92, 14730–14739
923 (2020).
924 64. Pineda, J. A. A. P. et al. Structural and functional analysis of female sex hormones
925 against SARS-Cov2 cell entry. bioRxiv (2020).
926 65. Gao, C. et al. SARS-CoV-2 Spike Protein Interacts with Multiple Innate Immune
927 Receptors. bioRxiv (2020) doi:10.1101/2020.07.29.227462.
928 66. Zhou, D., Tian, X., Qi, R., Peng, C. & Zhang, W. Identification of 22 N-glycosites
929 on spike glycoprotein of SARS-CoV-2 and accessible surface glycopeptide motifs:
930 Implications for vaccination and antibody therapeutics. Glycobiology 31, 69–80 (2021).

67. Casalino, L. et al. Beyond shielding: The roles of glycans in the SARS-CoV-2 spike protein. ACS Cent. Sci. 6, 1722–1734 (2020).
68. Zhang, L. et al. Furin cleavage of the SARS-CoV-2 spike is modulated by O-glycosylation. bioRxiv 2021.02.05.429982 (2021).
69. Henderson, R. et al. Controlling the SARS-CoV-2 spike glycoprotein conformation. Nat. Struct. Mol. Biol. 27, 925–933 (2020).
70. Shajahan, A., Supekar, N. T., Gleinich, A. S. & Azadi, P. Deducing the N- And O-glycosylation profile of the spike protein of novel coronavirus SARS-CoV-2. Glycobiology 30, 981–988 (2020).
71. Zhao, P. et al. Virus-Receptor Interactions of Glycosylated SARS-CoV-2 Spike and Human ACE2 Receptor. Cell Host Microbe 28, 586-601.e6 (2020).
72. Yang, Q. et al. Inhibition of SARS-CoV-2 viral entry in vitro upon blocking N- and O-glycan elaboration. bioRxiv 1–19 (2020) doi:10.1101/2020.10.15.339838.
73. Dawood, A. A. & Altobje, M. A. Inhibition of N-linked Glycosylation by Tunicamycin May Contribute to The Treatment of SARS-CoV-2. Microb. Pathog. 149, 104586 (2020).
74. Boson, B. et al. The SARS-CoV-2 envelope and membrane proteins modulate maturation and retention of the spike protein, allowing assembly of virus-like particles. J. Biol. Chem. 296, 100111 (2021).
75. Li, Q. et al. The Impact of Mutations in SARS-CoV-2 Spike on Viral Infectivity and Antigenicity. Cell 182, 1284-1294.e9 (2020).
76. Mohammad, S. et al. Sars-cov-2 orf8 and sars-cov orf8ab: Genomic divergence and functional convergence. Pathogens 9, 1–26 (2020).
77. Li, J. et al. The ORF6, ORF8 and nucleocapsid proteins of SARS-CoV-2 inhibit type Iinterferon signaling pathway. Virus Res. 286, (2020).
78. Zhang, Y. et al. The ORF8 protein of SARS-CoV-2 mediates immune evasion through potently downregulating MHC-I. bioRxiv (2020) doi:10.1101/2020.05.24.111823.
79. Hachim, A. et al. ORF8 and ORF3b antibodies are accurate serological markers of early and late SARS-CoV-2 infection. Nat. Immunol. 21, 1293–1301 (2020).
80. Shental-Bechor, D. & Levy, Y. Effect of glycosylation on protein folding: A close look at thermodynamic stabilization. Proc. Natl. Acad. Sci. U. S. A. 105, 8256–8261 (2008).
81. Adams, C. J., Kopp, M. C., Larburu, N., Nowak, P. R. & Ali, M. M. U. Structure and molecular mechanism of ER stress signaling by the unfolded protein response signal activator IRE1. Front. Mol. Biosci. 6, 1–12 (2019).
82. Casas-Sanchez, A. et al. Protein glycosylation is essential for SARS-CoV-2 infection. bioRxiv 2021.02.05.429940 (2021).
83. Ito, K. et al. Screening siRNAs against host glycosylation pathways to develop novel antiviral agents against hepatitis B virus. Hepatol. Res. 50, 1128–1140 (2020).
84. Manalo, R. V. M. & Medina, P. M. B. The endoplasmic reticulum stress response in disease pathogenesis and pathophysiology. Egypt. J. Med. Hum. Genet. 19, 59–68 (2018).
85. Bamberger, C. et al. The Host Interactome of Spike Expands the Tropism of SARS-CoV-2. bioRxiv 2021.02.16.431318 (2021).
86. Lynch, J. M. et al. A thrombospondin-dependent pathway for a protective ERstress response. 149, 1257–1268 (2012).
87. Zhang, H. J. et al. Epstein-Barr virus activates F-box protein FBXO2 to limit viral infectivity by targeting glycoprotein B for degradation. PLoS Pathog. 14, 1–22 (2018).
88. Chu, H. et al. Middle East respiratory syndrome coronavirus and bat coronavirus HKU9 both can utilize GRP78 for attachment onto host cells. J. Biol. Chem. 293, 11709–11726 (2018).

89. Fukushi, M. et al. Monitoring of S Protein Maturation in the Endoplasmic Reticulum by Calnexin Is Important for the Infectivity of Severe Acute Respiratory Syndrome Coronavirus. J. Virol. 86, 11745–11753 (2012).
90. Li, J. et al. Virus-Host Interactome and Proteomic Survey Reveal Potential Virulence Factors Influencing SARS-CoV-2 Pathogenesis. Med 2, 99-112.e7 (2021).
91. Minakshi, R. et al. The SARS coronavirus 3a protein causes endoplasmic reticulum stress and induces ligand-independent downregulation of the Type 1 interferon receptor. PLoS One 4, 1–10 (2009).
92. Chan, C.-P. et al. Modulation of the Unfolded Protein Response by the Severe Acute Respiratory Syndrome Coronavirus Spike Protein. J. Virol. 80, 9279–9287 (2006).
93. Wyler, E. et al. Transcriptomic profiling of SARS-CoV-2 infected human cell lines identifies HSP90 as target for COVID-19 therapy. iScience 24, (2021).
94. Puthalakath, H. et al. ER Stress Triggers Apoptosis by Activating BH3-Only Protein Bim. Cell 129, 1337–1349 (2007).
95. Marciniak, S. J. et al. CHOP induces death by promoting protein synthesis and oxidation in the stressed endoplasmic reticulum. Genes Dev. 18, 3066–3077 (2004).
96. Hetz, C., Zhang, K. & Kaufman, R. J. Mechanisms, regulation and functions of the unfolded protein response. Nat. Rev. Mol. Cell Biol. 21, 421–438 (2020).
97. Camini, F. C., da Silva Caetano, C. C., Almeida, L. T. & de Brito Magalhães, C. L. Implications of oxidative stress on viral pathogenesis. Arch. Virol. 162, 907–917 (2017).
98. Gong, G., Waris, G., Tanveer, R. & Siddiqui, A. Human hepatitis C virus NS5A protein alters intracellular calcium levels, induces oxidative stress, and activates STAT-3 and NF-κB. Proc. Natl. Acad. Sci. U. S. A. 98, 9599–9604 (2001).
99. Pahl, H. L. Signal transduction from the endoplasmic reticulum to the cell nucleus. Physiol. Rev. 79, 683–701 (1999).
100. Berridge, M. J., Bootman, M. D. & Lipp, P. Calcium - a life and death signal. Nature 395, 645–648 (1998).
101. Tardif, K. D., Waris, G. & Siddiqui, A. Hepatitis C virus, ER stress, and oxidative stress. Trends Microbiol. 13, 159–163 (2005).
102. Li, S. et al. SARS-CoV-2 triggers inflammatory responses and cell death through caspase-8 activation. Signal Transduct. Target. Ther. 5, (2020).
103. Li, G. et al. Transcriptomic signatures and repurposing drugs for COVID-19 patients: findings of bioinformatics analyses. Comput. Struct. Biotechnol. J. 19, 1–15 (2021).
104. Islam, A. B. M. M. K. et al. Transcriptome of nasopharyngeal samples from COVID-19 patients and a comparative analysis with other SARS-CoV-2 infection models reveal disparate host responses against SARS-CoV-2. J. Transl. Med. 19, 1–25 (2021).
105. Krishnamoorthy, P., Raj, A. S., Roy, S. & Senthil, N. Comparative transcriptome analysis of SARS-CoV, MERS-CoV, and SARS-CoV-2 to identify potential pathways for drug repurposing. Comput. Biol. Med. 128, (2020).
106. Singh, K. et al. Network Analysis and Transcriptome Profiling Identify Autophagic and Mitochondrial Dysfunctions in SARS-CoV-2 Infection. Front. Genet. 12, 1–19 (2021).
107. Balakrishnan, B. & Lai, K. Modulation of SARS-CoV-2 Spike-induced Unfolded Protein Response (UPR) in HEK293T cells by selected small chemical molecules. bioaRxiv (2021) doi:10.1101/2021.02.04.429769.
108. Köseler, A., Sabirli, R., Gören, T., Türkçüer, I. & Kurt, Ö. Endoplasmic reticulum stress markers in SARS-COV-2 infection and pneumonia: Case-control study. In Vivo (Brooklyn). 34, 1645–1650 (2020).
109. Jin, J. et al. Reticulocalbin 3 deficiency in alveolar epithelium exacerbated bleomycin-induced pulmonary fibrosis. Am. J. Respir. Cell Mol. Biol. 59, 320–333 (2018).

110. Zhang, Q. et al. Rcn3 suppression was responsible for partial relief of emphysema as shown by specific type II alveolar epithelial cell Rcn3 CKO mouse model. Int. J. COPD 16, 147–158 (2021).
111. Li, G. et al. Role of ERO1-α-mediated stimulation of inositol 1,4,5-triphosphate receptor activity in endoplasmic reticulum stress-induced apoptosis. J. Cell Biol. 186, 783–792 (2009).
112. Yao, Y. et al. A non-canonical pathway regulates ER stress signaling and blocks ER stress-induced apoptosis and heart failure. Nat. Commun. 8, (2017).
113. Gu, Y. et al. The deubiquitinating enzyme UCHL1 negatively regulates the immunosuppressive capacity and survival of multipotent mesenchymal stromal cells article. Cell Death Dis. 9, (2018).
114. Shen, H., Sikorska, M., Leblanc, J., Walker, P. R. & Liu, Q. Y. Oxidative stress regulated expression of Ubiquitin Carboxyl-terminal Hydrolase-L1: Role in cell survival. Apoptosis 11, 1049–1059 (2006).
115. Tangri, A. et al. Deubiquitinase UCHL1 Maintains Protein Homeostasis through the PSMA7–APEH–Proteasome Axis in High-grade Serous Ovarian Carcinoma. Mol. Cancer Res. 1–15 (2021) doi:10.1158/1541-7786.mcr-20-0883.